Available online at www.sciencedirect.com
SCIENCE DIRECT®
Journal of Solid State Chemistry 178 (2005) 2050–2061
JOURNAL OF SOLID STATE CHEMISTRY
www.elsevier.com/locate/jssc

Oxygen ionic and electronic transport in apatite-type $La_{10-x}(Si,Al)_6O_{26\pm\delta}$

A.L. Shaula[a], V.V. Kharton[a,b,*], F.M.B. Marques[a]

[a]Department of Ceramics and Glass Engineering, CICECO, University of Aveiro, 3810-193 Aveiro, Portugal
[b]Institute of Physicochemical Problems, Belarus State University, 14 Leningradskaya Str., 220050 Minsk, Belarus

Received 4 January 2005; received in revised form 7 April 2005; accepted 14 April 2005

Abstract

The main factor governing the oxygen ionic conductivity in apatite-type $La_{10-x}Si_{6-y}Al_yO_{27-3x/2-y/2}$ ($x = 0-0.33$; $y = 0.5-1.5$) is the concentration of mobile interstitials determined by the total oxygen content. The ion transference numbers, measured by modified faradaic efficiency technique, vary in the range 0.9949–0.9997 in air and increase on reducing oxygen partial pressure due to decreasing p-type electronic conduction. The activation energies for ionic and hole transport are (56–67) $\pm$ 3 kJ/mol and (57–100) $\pm$ 8 kJ/mol, respectively. Increasing oxygen content leads to higher hole conduction in oxidizing atmospheres and promotes minor oxygen losses from the lattice when the oxygen pressure decreases, although the overall level of ionic conductivity is almost constant in the $p(O_2)$ range from 50 kPa down to 10^{-16} Pa. Under reducing conditions at temperatures above 1100 K, silicon oxide volatilization from the surface layers of apatite ceramics results in a moderate decrease of the conductivity with time. This suggests that the operation of electrochemical cells with silicate-based solid electrolytes should be limited to the intermediate-temperature range, such as 800–1000 K, where the ionic transport in most-conductive apatite phases containing 26.50–26.75 oxygen atoms per unit formula is higher than that in stabilized zirconia. The average thermal expansion coefficients of apatite ceramics, calculated from dilatometric data in air, are $(8.7–10.8) \times 10^{-6}\,K^{-1}$ at 300–1300 K.

Keywords: Lanthanum silicate; Apatite; Solid oxide electrolyte; Oxygen ionic conductivity; Electronic transport; Faradaic efficiency; Ion transference number; Thermal expansion; Seebeck coefficient

1. Introduction

Oxygen ion-conducting solid electrolytes are key materials for numerous high-temperature electrochemical applications, such as solid oxide fuel cells (SOFCs), gas electrolyzers, oxygen sensors, and electrocatalytic reactors for natural gas conversion [1–3]. These electrochemical technologies provide important advantages with respect to conventional industrial processes. In particular, the use of SOFCs for electric power generation is characterized by a high energy-conversion efficiency, environmental safety and fuel flexibility including the prospects of direct operation with natural gas. Practical application of SOFCs is, however, still limited due to high costs of the component materials and processing. The SOFC-based systems are expected to become commercially feasible when their costs decrease several times, down to approximately 0.7 US$/W [2,3]. Developments of novel oxygen ion-conducting materials, in particular solid electrolytes, are therefore of vital importance in this field.

Recently, a substantial level of oxygen ionic conductivity has been reported for phases derived from apatite-type silicates and germanates with general formula $A_{10-x}(MO_4)_6O_{2\pm\delta}$ (M = Si, Ge), where A are

*Corresponding author. Present address: Department of Ceramics and Glass Engineering, CICECO, University of Aveiro, 3810-193 Aveiro, Portugal. Fax: +351 234 425300.
E-mail address: kharton@cv.ua.pt (V.V. Kharton).

0022-4596/$ - see front matter © 2005 Elsevier Inc. All rights reserved.
doi:10.1016/j.jssc.2005.04.018

rare- and alkaline-earth cations [4–17]. The apatite lattice tolerance with respect to *A*-site deficiency and to extensive aliovalent doping provides a possibility for further optimization of transport properties of these solid electrolytes. The ionic conduction in $Re_{10-x}Si_6O_{26+\delta}$ (Re = La–Yb; $x = 0-0.67$) increases with increasing radius of Re^{3+} cations, whilst the activation energy decreases; maximum conductivity is characteristic of the La-containing silicates [4,5,7,16]. Similar correlation is well known for perovskite- and K_2NiF_4-type oxides [18]. As for the *A*-site cation radii, the larger size of Ge^{4+} with respect to Si^{4+} results in a higher conductivity for Ge-based apatites compared to analogous silicates, although the activation energies of the former compounds are typically higher [6,15]. However, the Ge-containing materials suffer from Ge volatility and possible transformation into La_2GeO_5 at high temperatures, necessary to sinter dense ceramics [13,15].

The apatite lattice consists of a network of isolated MO_4 tetrahedra creating cavities occupied by *A*-site cations; additional oxygen sites surrounded by the *A*-site ions form channels running through the structure along the *c*-axis. The conductivity data on apatite single crystals, and the results of atomistic modelling, structural refinement and Mössbauer spectroscopy ([7,11–14] and references therein) clearly showed that interstitial migration along these channels has a key contribution to the overall level of ionic transport. Particular consequences include anisotropy of oxygen ion diffusivity, which is essentially higher in the direction parallel to the c-axis, and a decrease of ionic conductivity on decreasing oxygen content, especially below 26 oxygen atoms per apatite unit formula [8,9,12,13,16,17]. The maximum ionic conduction might therefore be expected for $La_{10}Si_6O_{27}$. At the same time, the existence of this phase under equilibrium conditions at SOFC operation temperatures is still questionable [5,8-10]. Although no phase impurities are often indicated in $Re_{10}M_6O_{27}$ ceramics by X-ray diffraction (XRD) analysis [6,9], grain-boundary studies, using electron microscopy, are necessary to confirm the existence of apatites with high oxygen excess as equilibrium phases and the absence of phase segregation. Another important factor affecting ionic transport in the apatite lattice relates to the *A*-site vacancies, particularly in positions enveloping oxygen channels. The *A*-site deficiency influences the SiO_4 tetrahedra relaxation and may cause displacement of the anions from channels into new interstitial sites, thus creating vacancies at fixed oxygen content [10,11,14,16]. For instance, an enhancement of the ionic transport is obtained in the $La_{9.33+x/3}Si_{6-x}Al_xO_{26}$ series, where Al doping is compensated by *A*-site vacancies without oxygen content variations, with maximum conductivity for $x = 1.5$ [10]. The information on electronic conduction in apatite-type silicates is scarce.

This work is focused on the study of $La_{10-x}Si_{6-y}Al_yO_{27-3x/2-y/2}$ ($x = 0-0.33$; $y = 0.5-1.5$) solid electrolytes, with particular emphasis on the properties most relevant for practical applications, namely the partial ionic and electronic conductivities, transference numbers, thermal expansion and stability at low oxygen partial pressures.

2. Experimental

Dense ceramic samples of $La_{10-x}Si_{6-y}Al_yO_{27-3x/2-y/2}$ ($x = 0$, 0.17 and 0.33; $y = 0.5$, 1.0 and 1.5) were prepared by the standard solid-state technique from high-purity La_2O_3, SiO_2 and $Al(NO_3)_3 \cdot 9H_2O$. Before weighting, lanthanum oxide and silica were annealed in air at 1473 and 873 K, respectively. The stoichiometric mixtures were calcined in air at 1023 K for 2 h, ball-milled, and reacted at 1273–1473 K in air. Then the powders were ball-milled again and uniaxially pressed into disks of various thickness at 120–250 MPa. Gas-tight ceramics were sintered at 1923–1973 K during 10 h in air. In all cases, the density of materials was higher than 91% of their theoretical density calculated from XRD data (Table 1).

The XRD patterns were collected at room temperature using a Rigaku D/MAX-B diffractometer (Cu$K\alpha$, $2\Theta = 10-100^\circ$, step 0.02°, 1 s/step); the structural parameters were refined employing the Fullprof program [19]. A Linseis L70 dilatometer (heating rate of 5 K/min) was used to study thermal expansion in air. Microstructure was examined using a Hitachi S-4100 scanning electron microscope (SEM) with a Rontec UHV Detection system for the energy dispersive spectroscopy (EDS). The temperature dependencies of the total conductivity (σ) in flowing air, argon and 10%H_2–90%N_2 mixture were measured by AC impedance spectroscopy (HP4284A precision LCR meter, 20 Hz–1 MHz); the oxygen partial pressure in the measuring cell was determined using an yttria-stabilized zirconia (YSZ) oxygen sensor. The values of the activation energy (E_a) were calculated by the standard Arrhenius equation

$$\sigma = \frac{A_0}{T}\exp\left[-\frac{E_a}{RT}\right], \quad (1)$$

where A_0 is the pre-exponential factor. The isothermal measurements of the total conductivity and Seebeck coefficient at 973–1223 K were carried out in the oxygen partial pressure range 1×10^{-16} to 5×10^4 Pa as described elsewhere [20,21]. The oxygen ion transference numbers were determined by the modified faradaic efficiency (FE) technique, taking electrode polarization into account [22]. In combination with the use of electrodes having a relatively high polarization resistance, this method enables to significantly improve the

Table 1
Properties of apatite ceramics

Composition	Space group	Unit cell parameters		Relative density (%)	Average TECs	
		a (Å)	c (Å)		T (K)	$\bar{\alpha} \times 10^6$ (K^{-1})
$La_{9.67}Si_{4.5}Al_{1.5}O_{25.75}$	$P\bar{3}$ (No 147)	9.733(3)	7.235(6)	96.7	373–1173	9.99±0.01
$La_{9.67}Si_5AlO_{26}$	$P6_3$ (No 173)	9.732(1)	7.223(6)	97.4	373–1173	9.92±0.01
$La_{9.67}Si_{5.5}Al_{0.5}O_{26.25}$	$P6_3/m$ (No 176)	9.712(2)	7.207(6)	93.8	373–1273	9.39±0.02
$La_{9.83}Si_{4.5}Al_{1.5}O_{26}$	$P\bar{3}$ (No 147)	9.734(3)	7.236(6)	96.7	373–1173	8.86±0.02
$La_{9.83}Si_{5.5}Al_{0.5}O_{26.5}$	$P6_3/m$ (No 176)	9.709(4)	7.207(9)	91.3	373–1273	10.80±0.02
$La_{10}Si_5AlO_{26.5}$	$P6_3/m$ (No 176)	9.729(5)	7.235(9)	91.6	473–1173	9.08±0.02
$La_{10}Si_{5.5}Al_{0.5}O_{26.75}$	$P6_3/m$ (No 176)	9.716(5)	7.212(7)	90.5	1173–1323	8.68±0.01

Composition	Ion transference numbers in air				Activation energies[a] (kJ/mol)	
	1223 K	1123 K	1073 K	973 K	Ion transport	Hole transport
$La_{9.67}Si_{4.5}Al_{1.5}O_{25.75}$	—	—	—	—	60±1	—
$La_{9.67}Si_5AlO_{26}$	0.9959	0.9959	0.9964	0.9965	67±1	72±3
$La_{9.67}Si_{5.5}Al_{0.5}O_{26.25}$	0.9956	0.9962	0.9966	0.9979	63±2	89±8
$La_{9.83}Si_{4.5}Al_{1.5}O_{26}$	0.9949	0.9951	0.9951	0.9948	60±2	57±2
$La_{9.83}Si_{5.5}Al_{0.5}O_{26.5}$	0.9967	0.9975	0.9982	0.9989	57±3	100±6
$La_{10}Si_5AlO_{26.5}$	0.9959	0.9968	0.9975	0.9985	56±3	96±6
$La_{10}Si_{5.5}Al_{0.5}O_{26.75}$	0.9995	0.9996	0.9996	0.9997	56±3	68±3

[a]The activation energies for ionic and hole conductivities correspond to the temperature ranges 873–1273 K and 973–1223 K, respectively.

accuracy of the determination of minor electronic contributions to the total conductivity [22]. The FE measurements were performed under zero oxygen chemical potential gradient in air at 973–1223 K, and also isothermally as a function of the oxygen partial pressure inside the cell (p_1) with constant oxygen pressure at the external electrode (p_2) equal to 0.21 atm (atmospheric air). In the latter case, the results were corrected for the oxygen permeation fluxes, determined prior to the measurement of each data point. All values of the transference numbers presented in this work were measured 2–5 times varying the current through sample; then the data points were averaged.

3. Results and discussion

3.1. General characterization

XRD analysis confirmed that all studied ceramic materials are single-phase; the lattice parameters and space groups are listed in Table 1. Incorporation of Al^{3+} having larger radius with respect to Si^{4+} increases the unit cell volume, analogously to doping with Fe^{3+}, Ga^{3+} and Ge^{4+} [12,14,15]. At fixed B-site composition, increasing A-site deficiency has an opposite effect, in agreement with data on $La_{10-x}Si_6O_{27-3x/2}$ [9].

The SEM/EDS studies showed high quality of the silicate ceramics, in particular low porosity and an absence of compositional inhomogeneities at the grain boundaries, within the limits of experimental uncertainty of the EDS technique. Typical SEM micrographs are presented in Fig. 1. The average grain size is quite similar for all ceramics and varies from 1 to 4 μm. The results of SEM/EDS inspections agree well with the impedance spectroscopy data (Fig. 2), which suggest no considerable grain-boundary contribution to the total resistivity at temperatures above 873–923 K. The impedance spectra consisted of one or two arcs. In the first case, the high- and low-frequency intercepts on the real axis correspond to the total resistance of a sample and the DC resistance of the cell, respectively. In the second case, the high-frequency arc can be approximated by a resistance-capacitance (RC) element; the deviation of the high-frequency intercept from origin was found negligible, within the limits of experimental error. For such spectra, the total conductivity can be calculated from the intermediate-frequency intercept. Due to the limited range of frequencies used in this work (20 Hz–1 MHz), only a part of these arcs is often visible in the impedance spectra; nonetheless, these are sufficient to separate total resistivity of the materials and to ensure the absence of grain-boundary signal.

The dilatometric curves of $La_{10-x}Si_{6-y}Al_yO_{27-3x/2-y/2}$ in air are approximately linear within the studied temperature range (Fig. 3). The average thermal expansion coefficients (TECs) calculated from the dilatometric data are relatively low, 8.7×10^{-6} to $10.8 \times 10^{-6}\,K^{-1}$ (Table 1). These values are close to

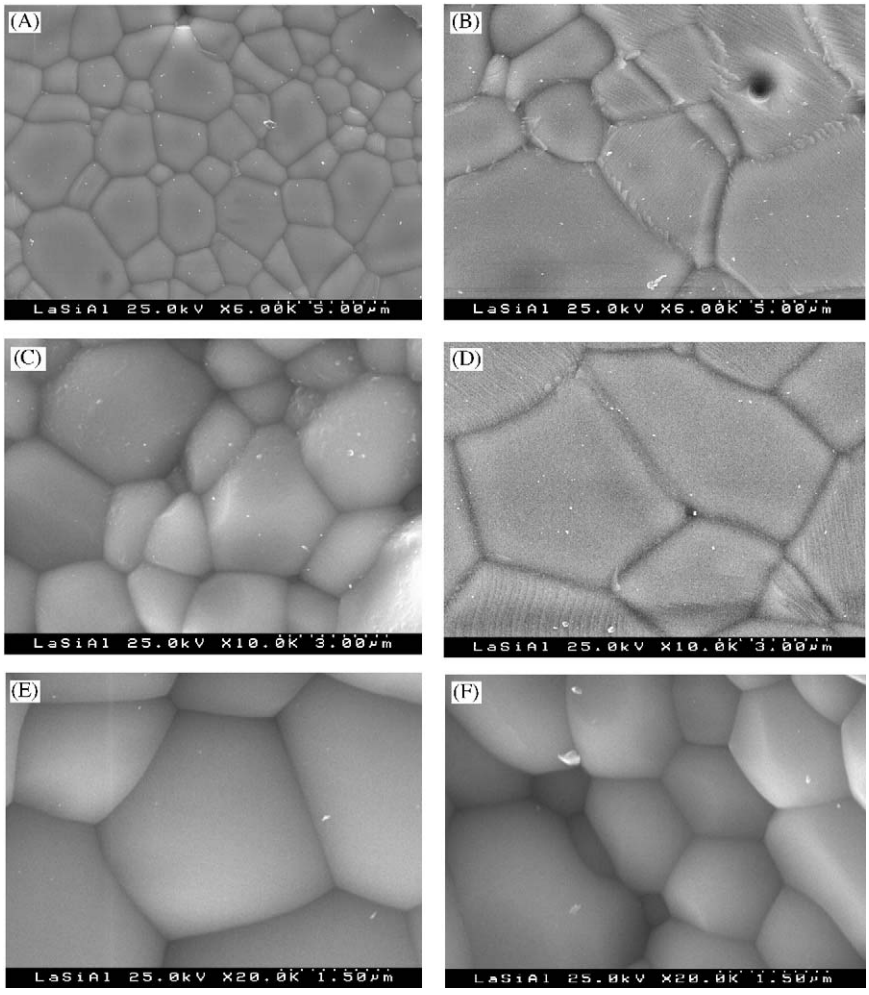

Fig. 1. SEM micrographs of apatite ceramics: $La_{9.67}Si_{5.5}Al_{0.5}O_{26.25}$ (A), $La_{10}Si_{5.5}Al_{0.5}O_{26.75}$ (B), $La_{9.83}Si_{4.5}Al_{1.5}O_{26}$ (C), $La_{9.83}Si_{5.5}Al_{0.5}O_{26.5}$ (D), $La_{9.67}Si_{4.5}Al_{1.5}O_{25.75}$ (E) and $La_{9.67}Si_5AlO_{26}$ (F).

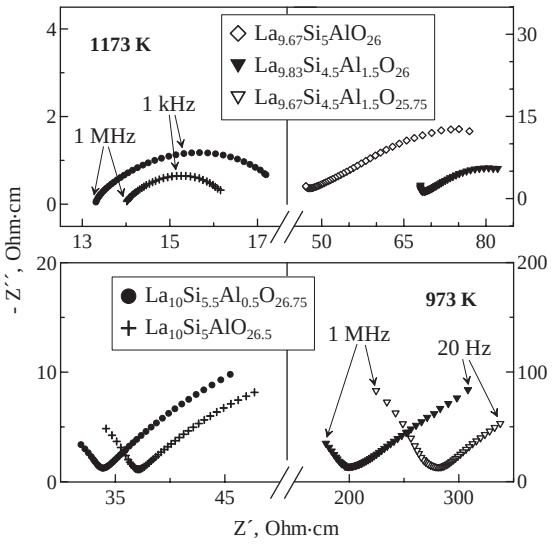

Fig. 2. Examples of the impedance spectra of $La_{10-x}Si_6O_{27-3x/2}$ ceramics with porous Pt electrodes in air.

those of commonly used solid electrolytes and electrode materials, such as stabilised zirconia [23] and lanthanum–strontium manganites [24].

3.2. Ionic conduction

The FE measurements clearly demonstrated that $La_{10-x}Si_{6-y}Al_yO_{27-3x/2-y/2}$ are oxygen ion-conducting solid electrolytes. At 973–1223 K in air, the electronic contribution to the total conductivity is about 0.5% or lower (Table 1). The Arrhenius plots of the conductivity, predominantly ionic, are shown in Fig. 4. The activation energy for ionic transport is relatively low and varies in the range 56–67 kJ/mol (Table 1).

The fact that the oxygen ionic conduction in the title materials dominates, was confirmed by data on oxygen pressure dependencies of total conductivity and Seebeck coefficient (α). One representative example is given in Fig. 5. The conductivity is almost $p(O_2)$-independent,

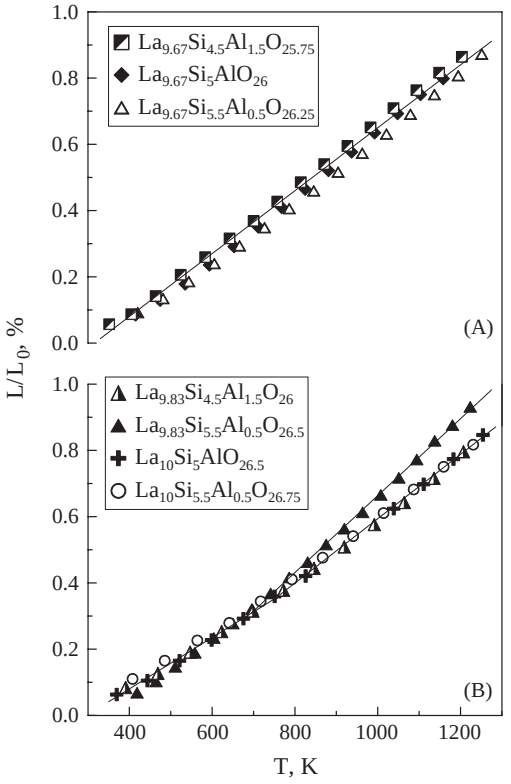

Fig. 3. Dilatometric curves of apatite ceramics in air.

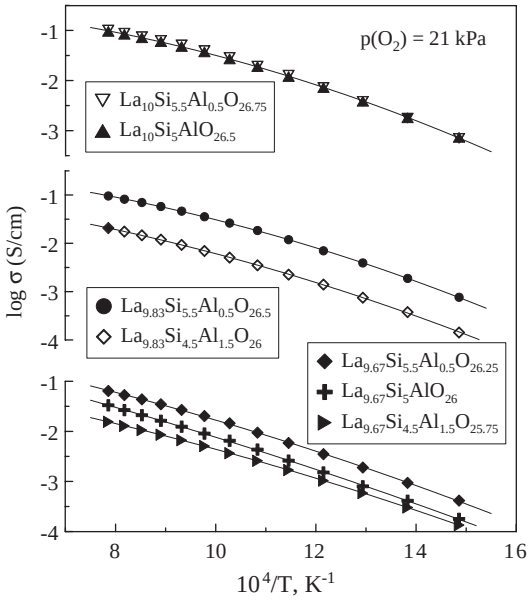

Fig. 4. Temperature dependence of the total conductivity of apatite ceramics in air. Solid lines are for visual guidance only.

while the thermopower under oxidizing conditions is positive; the slope of the α vs. $\ln p(O_2)$ dependencies is close to $-R/4F$, the theoretical value for a pure oxygen ionic conductor where the partial molar entropy and the transported heat of oxygen ions are both $p(O_2)$-

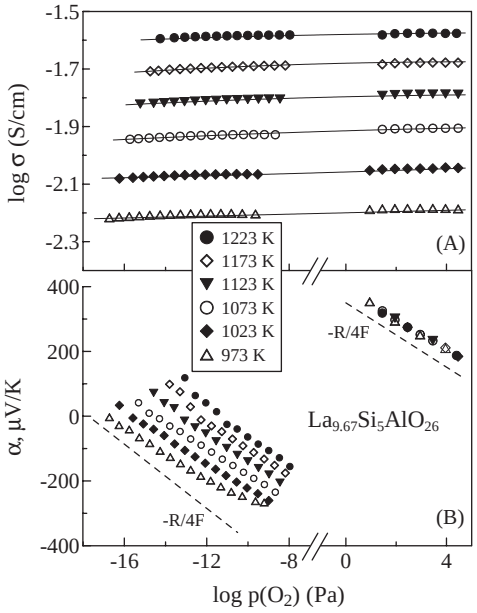

Fig. 5. Oxygen pressure dependencies of total conductivity (A) and Seebeck coefficient (B) of $La_{9.67}Si_5AlO_{26}$ ceramics.

independent [25]. This type of behavior is typical for solid electrolytes, such as stabilized zirconia [25,26]. Note that, in Fig. 5, the range of moderately low oxygen pressures is excluded from consideration due to errors in the oxygen sensor readings, associated with stagnated diffusion processes in the gas phase.

The oxygen ionic transport was found to increase with increasing oxygen content in the apatite lattice (Fig. 4); the highest conductivity is characteristic of silicate compositions containing 26.25–26.75 oxygen atoms per formula unit. These results corroborate that migration of interstitial O^{2-} is a major mechanism for ionic conductivity in apatites with relatively high oxygen concentration, in agreement with literature [9,11,12,16,17]. Note also that the diffusion of interstitial oxygen is expected to be significantly faster than that of the oxygen vacancies [11,12]. At the same time, the vacancy formation due to Frenkel-type disorder in the oxygen sublattice may still play an important role, enabling ion jumps between interstitial and regular sites. Such a disorder, and also SiO_4 tetrahedra relaxation are both promoted by the *A*-site deficiency [10,11,13]. This explains moderate differences in the ionic conductivity of compositions where the nominal oxygen content is similar, but the concentrations of *A*-site cation vacancies are different (Fig. 4).

The solid electrolytes of $La_{10-x}Si_{6-y}Al_yO_{27-3x/2-y/2}$ series, which contain 26.50–26.75 oxygen atoms per formula unit, exhibit a level of oxygen ionic transport comparable to that of yttria-stabilized zirconia, especially at temperatures below 1100 K (Fig. 6). These values are substantially higher with respect to the ionic conductivity of $Gd_{1.8}Ca_{0.2}Ti_2O_{7-\delta}$ pyrochlore, another

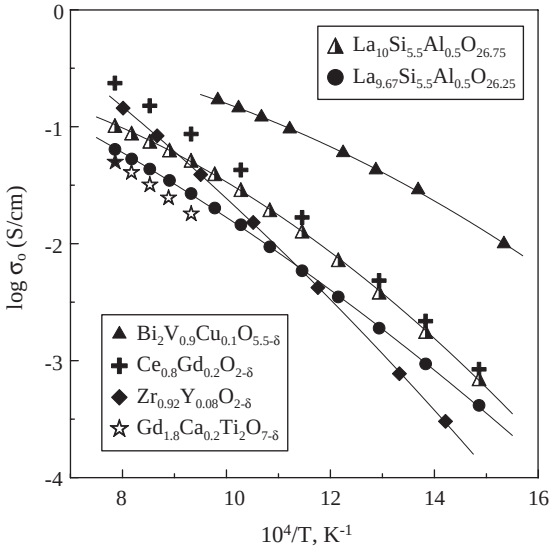

Fig. 6. Temperature dependence of the oxygen ionic conductivity of various solid electrolytes in air. Data on $Bi_2V_{0.9}Cu_{0.1}O_{5.5-\delta}$ [27], $Ce_{0.8}Gd_{0.2}O_{2-\delta}$ [22], yttria-stabilized zirconia [28] and $Gd_{1.8}Ca_{0.2}Ti_2O_{7-\delta}$ [29] are shown for comparison.

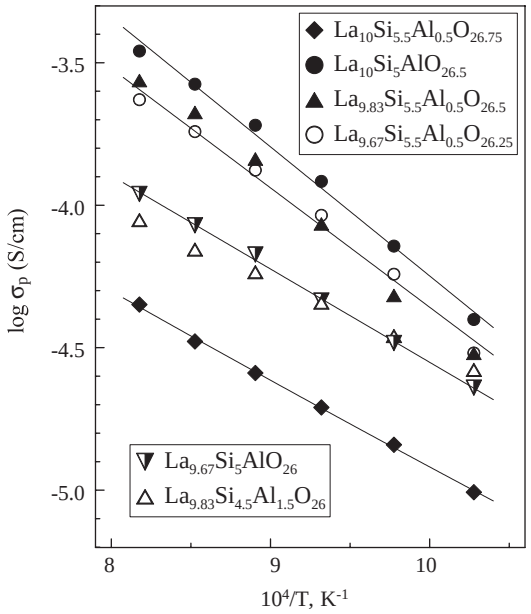

Fig. 7. Temperature dependence of the partial p-type electronic conductivity of apatite ceramics in air.

interesting electrolyte [29]. At 770–870 K, the conductivity of $La_{10}Si_{5.5}Al_{0.5}O_{26.75}$ is quite close to that of 20% gadolinia-doped ceria (CGO). Notice that the latter is among the most promising candidates for intermediate-temperature (IT) SOFCs; in spite of relatively narrow electrolytic domain, the use of CGO at $T < 1000$ K is considered feasible [2]. Although this level of ionic conduction is lower than that for Bi_2O_3-based electrolytes such as $Bi_2V_{0.9}Cu_{0.1}O_{5.5-\delta}$ (so-called BICUVOX), the use of Bi-containing materials for SOFCs is hampered due to their low stability in reducing atmospheres [27]. Compared to $LaGaO_3$-based solid electrolytes, having a conductivity close to that of CGO, the cost of doped lanthanum silicates is substantially lower. In addition, the technologies for SiO_2-based film processing, well developed in the electronic industry, can be adopted for fabrication of planar electrochemical cells with silicate-based electrolytes. Most conductive lanthanum silicate-based materials, such as $La_{10}Si_{5.5}Al_{0.5}O_{26.75}$, can therefore be considered for applications in IT SOFCs.

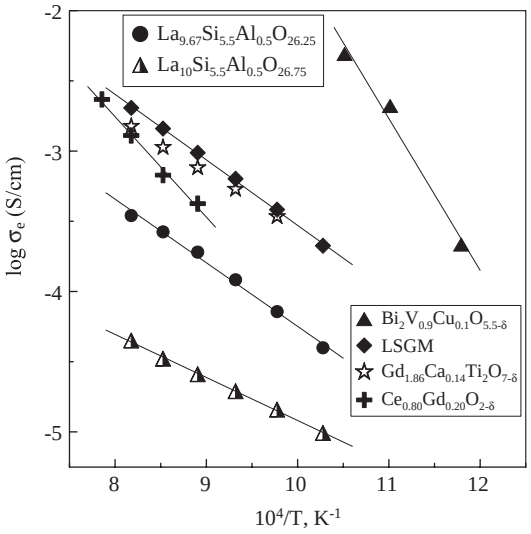

Fig. 8. Total electronic (p- and n-type) conductivity of various solid electrolytes in oxidizing conditions. Data on $(La_{0.9}Sr_{0.1})_{0.98}Ga_{0.8}Mg_{0.2}O_{3-\delta}$ (LSGM) [31], CGO [22] and $Gd_{1.86}Ca_{0.14}Ti_2O_{7-\delta}$ [30] correspond to $p(O_2) = 21$ kPa (atmospheric air). Data on $Bi_2V_{0.9}Cu_{0.1}O_{5.5-\delta}$ [27] correspond to the oxygen partial pressure gradient of 1.0/0.21 atm.

3.3. Electron–hole transport

Fig. 7 presents the temperature dependencies of the partial electronic conductivity, calculated from results of the impedance spectroscopy and FE measurements in air. The activation energy varies from 57 to 100 kJ/mol (Table 1). The relation between the E_a values for ionic and electronic conductivities determines the variations of transference numbers with temperature. As for doped $LaGaO_3$ [31] and CGO [21], the oxygen ion transference numbers of most silicates increase when temperature decreases, while the composition with maximum aluminum concentration, $La_{9.83}Si_{4.5}Al_{1.5}O_{26}$, exhibits the opposite behavior (Table 1). The latter trend is similar to $LaAlO_3$-based solid electrolytes [32,33]. The overall level of electronic conduction in the title materials, close to that of stabilized zirconia [23], is considerably lower with respect to $Bi_2VO_{5.5}$-, $LaGaO_3$-, $Gd_2Ti_2O_7$- and CeO_2-based solid electrolytes under oxidizing conditions (Fig. 8).

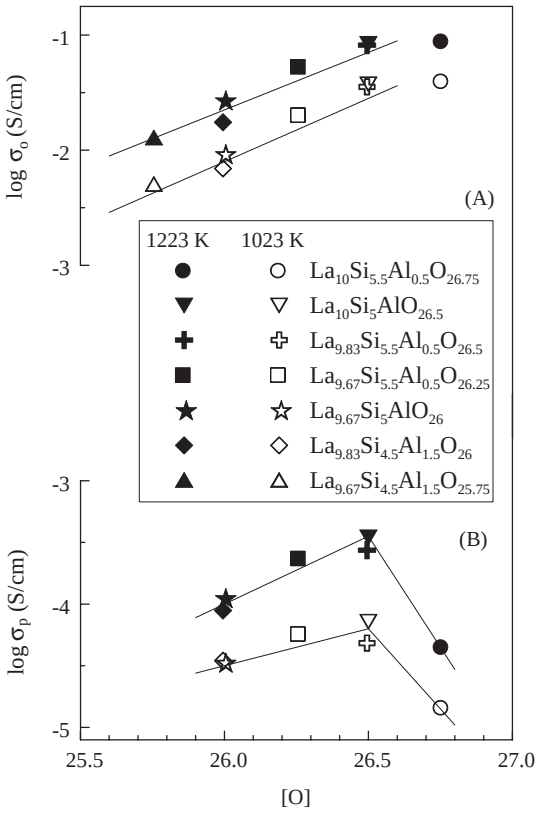

Fig. 9. Relationships between nominal oxygen content and partial ionic (A) and p-type electronic (B) conductivities of apatite ceramics in air.

One important tendency, earlier observed for Fe-substituted apatites [12], relates to the general correlation between total oxygen content, ionic transport and electronic conductivity (Fig. 9). The only exception is $La_{10}Si_{5.5}Al_{0.5}O_{26.75}$, the anomalous behavior of which may be caused either by local deviations from the nominal composition or by a change in the interstitials location due to high oxygen content, close to a possible maximum. For instance, contrary to *A*-site deficient $La_{9.83}Si_{4.5}Al_{1.5-y}Fe_yO_{26+\delta}$ where the interstitials are located in the vicinity of oxygen channels running through the lattice, $La_{10}Si_5FeO_{26.5}$ exhibits oxygen incorporation into the closest neighborhood of Si-site cations [12]. This assumption is in agreement with the tendency to plateau in the ionic conductivity vs. oxygen content curves (Fig. 9A).

In the case of iron doping, the correlation between ionic and electronic conductivities results from the oxygen intercalation process

$$\tfrac{1}{2}O_2 \rightarrow O_i'' + 2h^{\bullet} \qquad (2)$$

which increases the concentrations of oxygen interstitials and holes, both being the mobile charge carriers; the formation of Fe^{4+} due to hole localization on iron cations was verified by the Mössbauer spectroscopy [12]. A similar mechanism may also be expected for $La_{10-x}Si_{6-y}Al_yO_{27-3x/2-y/2}$. In the latter case, however, the lattice contains no variable-valence cations; the amount of hyperstoichiometric oxygen, which can be incorporated into the apatite structure in addition to the oxygen concentration determined by the cations charge, should be very small. One can expect, therefore, the presence of additional mechanism promoting generation of electronic charge carriers when the total oxygen content increases. As a hypothesis, one may suggest localization of the electronic charge carriers on lattice defects having opposite charge, similar to other solid electrolytes with perovskite- and fluorite-type structure [34]. In particular, the location of holes formed due to intrinsic electronic disorder ($0 \Leftrightarrow e' + h^{\bullet}$) is expected in the vicinity of O_i'' and Al′; the electrons may be localized on oxygen vacancies having effective positive charge. In this case, increasing concentration of interstitial oxygen should shift the electron-hole equilibrium towards hole formation. Although one could also expect an increase in the hole mobility and lower activation energy due to decreasing jump distance and, thus, lowering energetic barrier for hole transport when the oxygen content increases, this is not observed experimentally. In fact, the corresponding E_a values show a correlation similar to the variations of hole conductivity (σ_p), Fig. 10. Such tendency indicates that the migration energy becomes higher on increasing hole concentration, probably due to strong coulombic interaction between p-type electronic charge carriers. Note that the decrease of the ion transference numbers on increasing $p(O_2)$, Figs. 11 and 12, confirms that the electronic conduction in $La_{10-x}Si_{6-y}Al_yO_{27-3x/2-y/2}$ under oxidizing conditions is dominantly p-type.

When the concentration of mobile oxygen interstitials is high and essentially $p(O_2)$-independent, the

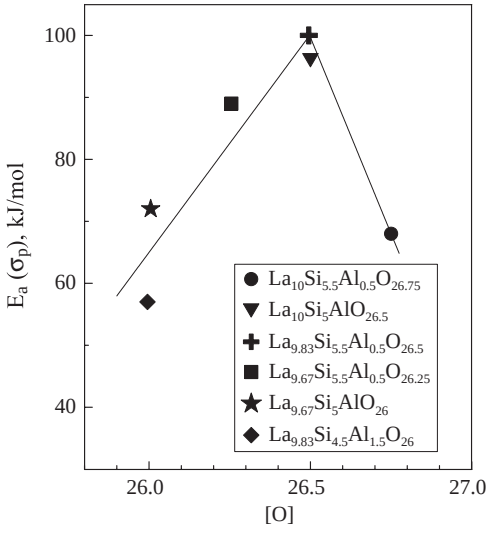

Fig. 10. Relationships between oxygen content and activation energy for the electron–hole conductivity of apatite ceramics.

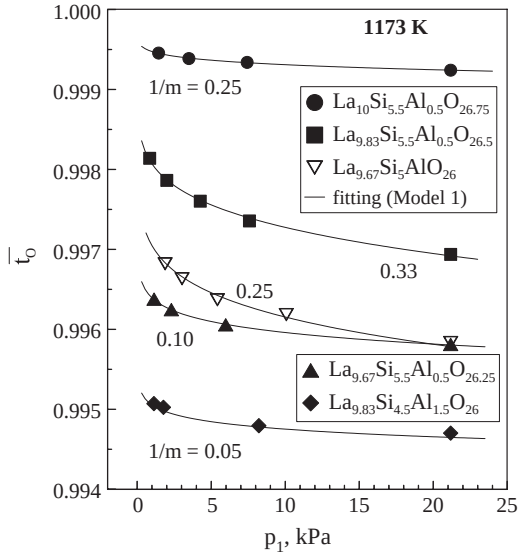

Fig. 11. Dependence of the average oxygen ion transference numbers of apatite ceramics, determined by FE measurements, on the oxygen partial pressure inside the measuring cells. Solid lines correspond to best fit Eq. (5).

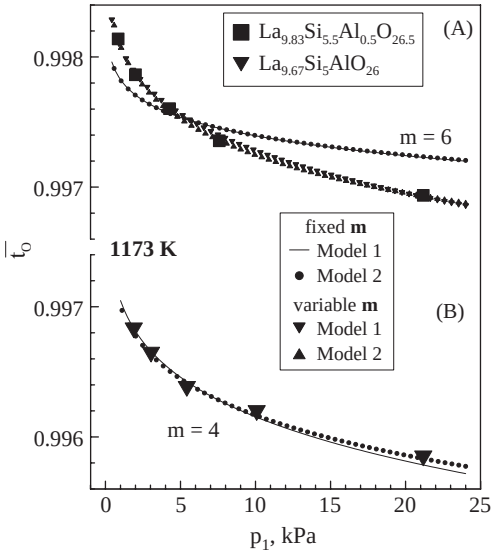

Fig. 12. Fitting results and experimental data on the average oxygen ion transference numbers of $La_{9.83}Si_{5.5}Al_{0.5}O_{26.5}$ and $La_{9.67}Si_5AlO_{26}$ vs. oxygen partial pressure inside the measuring cells (see text).

transference numbers under equilibrium conditions can be described assuming a power dependence of the p-type electronic conductivity on the oxygen partial pressure:

$$t_o = \frac{\sigma_o}{\sigma_o + \sigma_p^0 p(O_2)^{1/m}}, \tag{3}$$

where σ_o is the oxygen ionic conductivity, σ_p^0 is the p-type electronic conductivity at unit oxygen pressure, and m is a positive exponent. The theoretical value of m for solid electrolytes with $p(O_2)$-independent chemical potential of oxygen ions is 4. If the localization of holes on lattice point defects is significant, the exponent may achieve lower values [35]. Under non-zero gradient of oxygen chemical potential (μ), the measured transference numbers are average

$$\overline{t_o} = \frac{1}{\mu_2 - \mu_1}\int_{\mu_1}^{\mu_2} t_o \, d\mu, \tag{4}$$

where μ_1 and μ_2 are the chemical potentials corresponding to $p(O_2)$ values at the electrodes, p_1 and p_2. Substitution of Eq. (3) into Eq. (4) and consequent integration yield

$$\overline{t_o}(p_1, p_2) = -m \ln\frac{k_1 p_2^{-1/m} + 1}{k_1 p_1^{-1/m} + 1}\left(\ln\frac{p_2}{p_1}\right)^{-1}, \tag{5}$$

where $k_1 = \sigma_o/\sigma_p^0$. The fitting results using Eq. (5), below referred to as Model 1, are shown in Fig. 11 by solid lines. This formula describes adequately the observed $p(O_2)$ dependence of the oxygen ion transference numbers.

For $La_{9.67}Si_{5.5}Al_{0.5}O_{26.25}$ and $La_{9.83}Si_{4.5}Al_{1.5}O_{26}$, however, the variations of $\overline{t_o}$ are very small, less than 0.0005, although the average transference numbers still increase on reducing $p(O_2)$. Such a behavior may indicate either a significant concentration of n-type charge carriers, comparable to the hole concentration, or a substantial change in the mobile interstitials content according to Eq. (2). The total conductivity, predominantly ionic, indeed exhibits a slight decrease on reducing $p(O_2)$, Fig. 5. An oxygen pressure-dependent component was therefore added to the term of Eq. (3), describing the oxygen ionic conductivity:

$$t_o = \frac{\sigma_o^c + \sigma_o^0 p(O_2)^{1/m}}{\sigma_o^c + \sigma_o^0 p(O_2)^{1/m} + \sigma_p^0 p(O_2)^{1/m}}, \tag{6}$$

where σ_o^0 is the $p(O_2)$-dependent contribution to σ_0 at unit oxygen pressure, σ_o^c is the $p(O_2)$-independent contribution determined by the charge of cations constituting apatite lattice. Notice that the reaction expressed by Eq. (2) implies equal exponents for the power dependencies of point defect concentrations on the oxygen pressure. The last relationship gives another model for the ion transference numbers (Model 2):

$$\overline{t_o}(p_1, p_2) = 1 - m k_2 \ln\frac{k_3 p_2^{1/m} + 1}{k_3 p_1^{1/m} + 1}\left(\ln\frac{p_2}{p_1}\right)^{-1}, \tag{7}$$

where $k_2 = \sigma_p^0/(\sigma_o^0 + \sigma_p^0)$ and $k_3 = (\sigma_o^0 + \sigma_p^0)/\sigma_o^c$.

Fig. 12 compares the fitting results obtained using Models 1 and 2. For better visualization, the regression analysis was performed with both variable and fixed m; the theoretical values of $m = 4$ and 6 were chosen in the latter case. The results are clearly more adequate when m is equal to 4. Also, Model 2 provides a slightly better

description of the experimental data (Fig. 12B), thus suggesting a presence of small $p(O_2)$-dependent contribution to the ionic conductivity.

4. Behavior in reducing atmospheres

The impedance spectroscopy of $La_{10-x}Si_{6-y}Al_yO_{27-3x/2-y/2}$ ceramics in flowing air, argon and $10\%H_2$–$90\%N_2$ mixture showed that, on the contrary to Fe-containing apatites [12], only a minor decrease in ionic conduction is observed at low oxygen chemical potentials (Fig. 13). A similar conclusion was drawn analyzing the results of isothermal measurements of total conductivity vs. oxygen pressure (Fig. 14). The conductivity drop is more pronounced for the apatites with higher oxygen content, suggesting that increasing oxygen interstitial concentration leads to decreasing metal-oxygen bond strength and, hence, increases oxygen losses from the lattice. The maximum decrease of the conductivity is observed for $La_{10}Si_{5.5}Al_{0.5}O_{26.75}$. At $p(O_2) = 10^{-14}$–10^{-8} Pa, this composition exhibits a level of ionic transport lower than that of $La_{9.83}Si_{5.5}Al_{0.5}O_{26.5}$, although the nominal oxygen content in the former is higher. On cooling the conductivity changes become negligible; no changes in the σ values of $La_{10-x}Si_{6-y}Al_yO_{27-3x/2-y/2}$ on reducing oxygen pressure are observed below 1123 K. For the phases with relatively low oxygen content, such as $La_{9.83}Si_{4.5}Al_{1.5}O_{26}$, the conductivity is entirely $p(O_2)$-independent within all studied temperature range.

Neither segregation of secondary phases nor essential microstructural changes after treatment in reducing

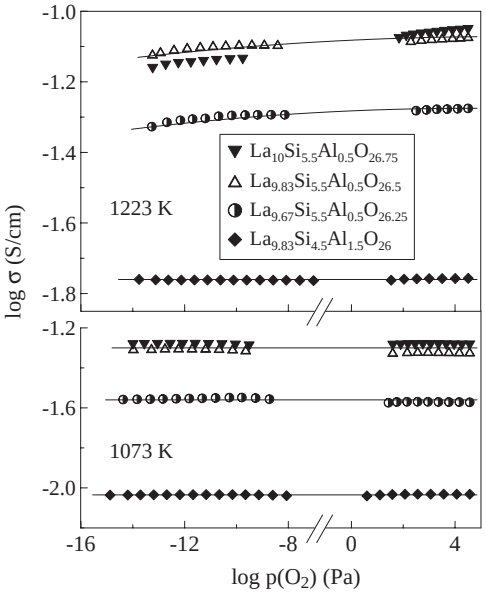

Fig. 14. Oxygen partial pressure dependencies of total conductivity of apatite ceramics.

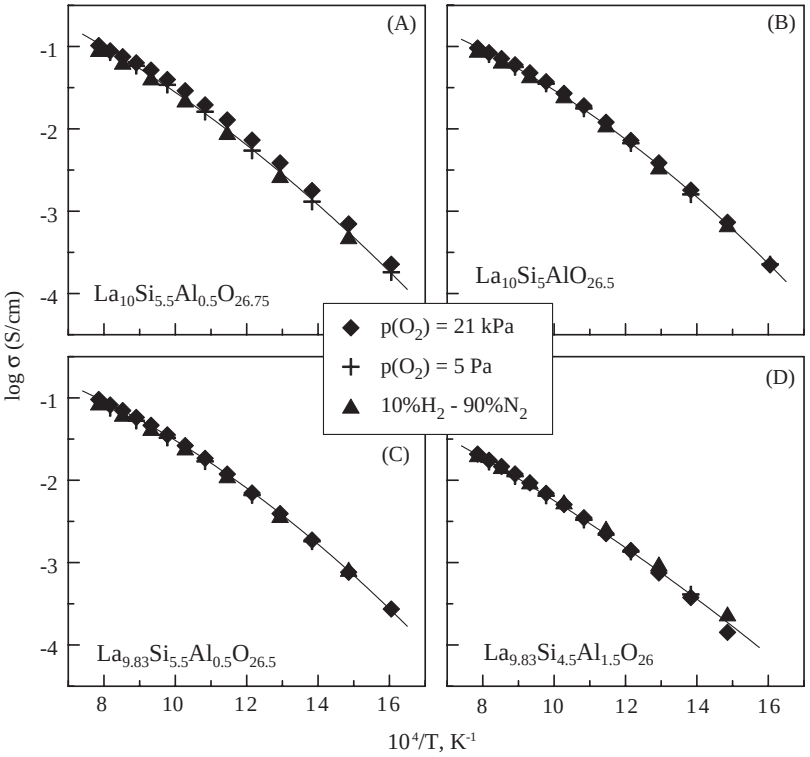

Fig. 13. Temperature dependence of the total conductivity of apatite ceramics in air, argon and dry $10\%H_2$–$90\%N_2$ atmospheres.

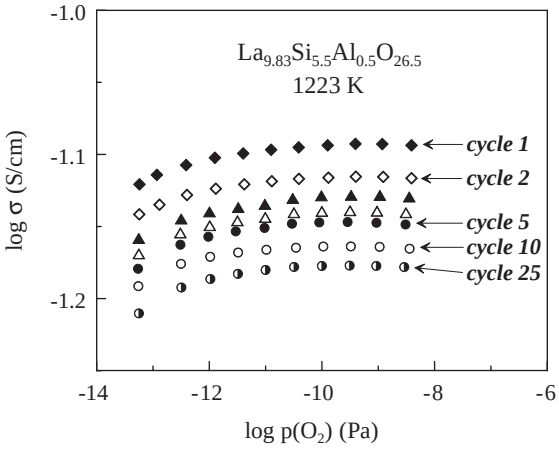

Fig. 15. Variations of the total conductivity of $La_{9.83}Si_{5.5}Al_{0.5}O_{26.5}$ ceramics in the course of cycling oxygen chemical potential under reducing conditions (see text). Duration of each cycle was 20–25 h. Data on 7 selected cycles are presented for clarity.

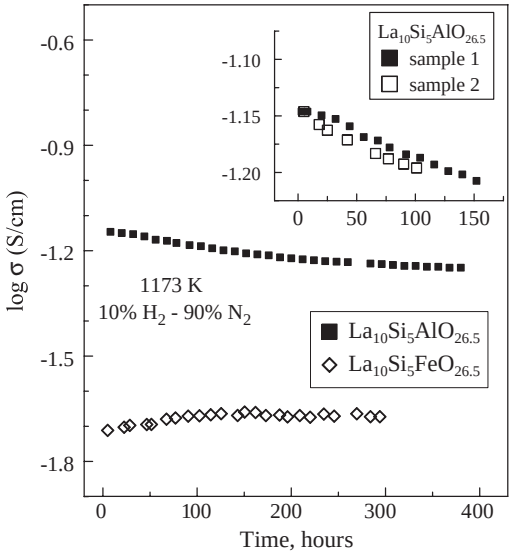

Fig. 16. Time dependencies of the total conductivity of apatite ceramics in flowing 10% H_2–90% N_2 mixture at 1173 K. Data on $La_{10}Si_5FeO_{26\pm\delta}$ apatite [12] are shown for comparison. Inset illustrates reproducibility of the conductivity variations for two similar samples.

atmospheres for 50–70 h was detected by XRD and SEM/EDS. The thermopower at low oxygen partial pressures becomes negative (Fig. 5), but its slope vs. $\ln p(O_2)$ is still close to the theoretical value for a pure oxygen-ionic conductor, $-R/4F$ [25]. The measurements of average ion transference numbers confirmed an absence of considerable n-type electronic contribution to the total conductivity at relatively low oxygen pressures. For example, the $\overline{t_o}$ value of $La_{9.67}Si_5AlO_{26}$ under air/10%H_2–90%N_2 gradient is about 0.999 at 1273 K.

However, the long-term stability tests in reducing gases demonstrated a slow irreversible degradation of silicate samples at temperatures above 1100 K, associated with minor volatilization of SiO from the surface layers of apatite ceramics. As an example, Fig. 15 shows the variations of total conductivity in the course of cycling oxygen partial pressure in CO–CO_2 atmosphere, using an electrochemical cell with oxygen pump and sensor [20]. Each data point was collected equilibrating the sample with the gas phase, until the conductivity relaxation rate after a change in the oxygen partial pressure became less than 0.05% per minute; the duration of each cycle was 20–35 h. After approximately 600 h, the conductivity of $La_{9.83}Si_{5.5}Al_{0.5}O_{26.5}$ ceramics at 1223 K decreased by 18% (Fig. 15). The maximum degradation was observed during first 120–150 h; subsequent annealing results in very small changes. Similar data were obtained in the course of long-term treatment in flowing H_2–N_2 gas mixture (Fig. 16). In this case, the conductivity drop for $La_{10}Si_5AlO_{26.5}$ ceramics at 1173 K is about 21%. The XRD analysis of the ceramics surface exposed to hydrogen-containing atmosphere during approximately 400 h, confirmed the presence of lanthanum oxide traces (Fig. 17). The secondary phase segregation at the surface is also visible in the SEM micrographs; one example is given in Fig. 18A. The XRD and SEM/EDS inspections of the ceramics bulk revealed no changes after long-term treatment in reducing environments, indicating that the conductivity variations with time are mainly related to surface layers. Note that, surprisingly, no conductivity degradation under identical conditions was found for iron-substituted apatites such as $La_{10}Si_5FeO_{26.5}$ [12], shown in Fig. 16 for comparison. Nonetheless, such treatment leads to significant changes in the surface morphology (Fig. 18B). Most likely, in the case of Fe-containing apatites, SiO volatilization is accompanied with surface reduction of iron into metal and/or formation of lanthanum ferrite phases having a relatively high n-type electronic conductivity, at the ceramics surface.

In general, although the time degradation of transport properties of $La_{10-x}Si_{6-y}Al_yO_{27-3x/2-y/2}$ materials in reducing environments is moderate, such a behavior is undesirable for practical applications such as SOFCs. In order to suppress silicon oxide volatilization from the surface layers of apatite ceramics, the operation temperature of electrochemical cells should be decreased down to 800–1000 K. This seems quite feasible, taking into account the relatively high ionic conductivity of the apatite phases with maximum oxygen content (Fig. 6).

5. Conclusions

Dense ceramics of apatite-type $La_{10-x}Si_{6-y}Al_yO_{27-3x/2-y/2}$ ($x = 0-0.33$; $y = 0.5-1.5$) were prepared via

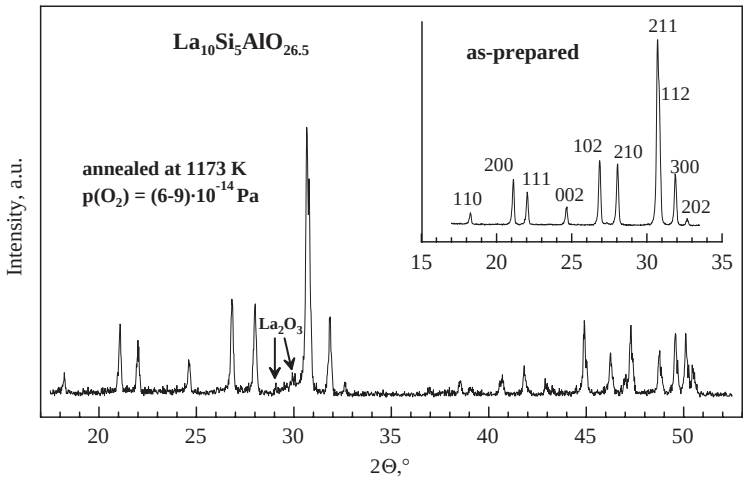

Fig. 17. XRD pattern of $La_{9.83}Si_{5.5}Al_{0.5}O_{26.5}$ ceramics surface after annealing in 10% H_2–90% N_2 mixture at 1173 K during 400 h. The strongest peaks of formed La_2O_3 phase are marked by arrows. The inset shows representative fragment of the XRD pattern of as-prepared material, with marked crystallographic indices.

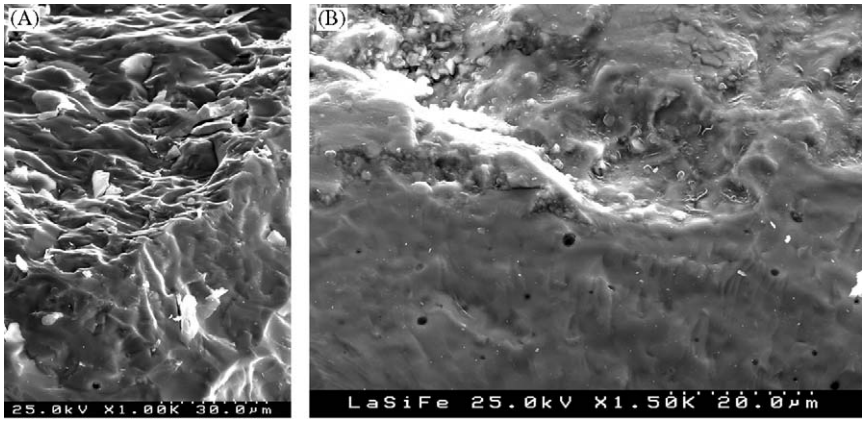

Fig. 18. SEM micrographs of $La_{9.83}Si_{5.5}Al_{0.5}O_{26.5}$ (A) and $La_{10}Si_5FeO_{26\pm\delta}$ (B) ceramics after annealing in 10% H_2–90% N_2 mixture at 1173 K during 300–400 h. Both micrographs show the surface exposed to H_2-containing atmosphere (top) and fractured bulk (bottom).

the standard solid-state synthesis route and characterized by XRD, SEM/EDS, dilatometry and the measurements of FE, total conductivity and Seebeck coefficient as function of the oxygen partial pressure. The oxygen ion transference numbers are higher than 0.995 in air and increase on reducing $p(O_2)$ due to decreasing p-type electronic conduction. The activation energies for ionic and hole transport vary in the ranges 56–67 and 57–100 kJ/mol, respectively. The main factor determining the level of ionic transport in $La_{10-x}Si_{6-y}Al_yO_{27-3x/2-y/2}$ apatites is the total oxygen content governed by cation composition. The maximum ionic conductivity, close to that of yttria-stabilized zirconia, was hence found for the phases containing 26.50–26.75 oxygen atoms per unit formula. At the same time, increasing oxygen content leads also to increasing hole conduction and decreasing metal-oxygen bond strength, thus promoting minor oxygen losses from the lattice when the oxygen partial pressure decreases. The average thermal expansion coefficients of apatite ceramics, $(8.7\text{-}10.8)\times10^{-6}\,K^{-1}$ at 300–1300 K, are similar to those of common solid-electrolyte materials. Despite silicon oxide volatilization from the surface layers under reducing conditions, which results in conductivity degradation with time at temperatures above 1100 K, the silicate-based solid electrolytes possess a promising combination of transport properties, thermal expansion and stability, enabling their use for IT SOFCs operating at 800–1000 K.

Acknowledgements

This work was supported by the FCT, Portugal (POCTI program and Project SFRH/BD/6595/2001) and the NATO Science for Peace program (project 978002).

References

[1] S.P.S. Badwal, F.T. Ciacchi, Adv. Mater. 13 (2001) 993.
[2] B.C.H. Steele, J. Mater. Sci. 36 (2001) 1053.
[3] O. Yamamoto, Electrochim. Acta 45 (2000) 2423.
[4] S. Nakayama, T. Kageyama, H. Aono, Y. Sadaoka, J. Mater. Chem. 5 (1995) 1801.
[5] S. Nakayama, M. Sakamoto, J. Eur. Ceram. Soc. 18 (1998) 1413.
[6] H. Arikawa, H. Nishiguchi, T. Ishihara, Y. Takita, Solid State Ionics 136-137 (2000) 31.
[7] S. Nakayama, M. Sakamoto, J. Mater. Sci. Lett. 20 (2001) 913.
[8] S. Nakayama, M. Sakamoto, J. Mater. Sci. Lett. 20 (2001) 1627.
[9] S. Tao, J.T.S. Irvine, Mater. Res. Bull. 36 (2001) 1245.
[10] E.J. Abram, D.C. Sinclair, A.R. West, J. Mater. Chem. 11 (2001) 1978.
[11] J.R. Tolchard, M.S. Islam, P.R. Slater, J. Mater. Chem. 13 (2003) 1956.
[12] V.V. Kharton, A.L. Shaula, M.V. Patrakeev, J.C. Waerenborgh, D.P. Rojas, N.P. Vyshatko, E.V. Tsipis, A.A. Yaremchenko, F.M.B. Marques, J. Electrochem. Soc. 151 (2004) A1236.
[13] J.R. Tolchard, J.E.H. Sansom, P.R. Slater, M.S. Islam, J. Solid State Electrochem. 8 (2004) 668.
[14] J.E.H. Sansom, J.R. Tolchard, P.R. Slater, M.S. Islam, Solid State Ionics 167 (2004) 17.
[15] J.E.H. Sansom, P.R. Slater, Solid State Ionics 167 (2004) 23.
[16] P.R. Slater, J.E.H. Sansom, Solid State Phenom 90-91 (2003) 195.
[17] S. Nakayama, Y. Higuchi, Y. Kondo, M. Sakamoto, Solid State Ionics 170 (2004) 219.
[18] V.V. Kharton, A.P. Viskup, A.V. Kovalevsky, E.N. Naumovich, F.M.B. Marques, Solid State Ionics 143 (2001) 337.
[19] J. Rodriguez-Carvajal, Physica B 192 (1993) 55.
[20] M.V. Patrakeev, E.B. Mitberg, A.A. Lakhtin, I.A. Leonidov, V.L. Kozhevnikov, V.V. Kharton, M. Avdeev, F.M.B. Marques, J. Solid State Chem. 167 (2002) 203.
[21] I.A. Leonidov, V.L. Kozhevnikov, E.B. Mitberg, M.V. Patrakeev, V.V. Kharton, F.M.B. Marques, J. Mater. Chem. 11 (2001) 1202.
[22] V.V. Kharton, A.P. Viskup, F.M. Figueiredo, E.N. Naumovich, A.A. Yaremchenko, F.M.B. Marques, Electrochim. Acta 46 (2001) 2879.
[23] V.V. Kharton, E.N. Naumovich, A.A. Vecher, J. Solid State Electrochem. 3 (1999) 61.
[24] V.V. Kharton, A.A. Yaremchenko, E.N. Naumovich, J. Solid State Electrochem. 3 (1999) 303.
[25] E. Ahlgren, F.W. Poulsen, Solid State Ionics 70-71 (1994) 528.
[26] S. Yamaguchi, K. Kobayashi, K. Abe, S. Yamazaki, Y. Iguchi, Solid State Ionics 113-115 (1998) 393.
[27] A.A. Yaremchenko, M. Avdeev, V.V. Kharton, A.V. Kovalevsky, E.N. Naumovich, F.M.B. Marques, Mater. Chem. Phys. 77 (2002) 552.
[28] M. Mori, T. Abe, H. Itoh, O. Yamomoto, Y. Takeda, T. Kawahara, Solid State Ionics 74 (1994) 157.
[29] S.A. Kramer, H.L. Tuller, Solid State Ionics 82 (1995) 15.
[30] V.V. Kharton, E.V. Tsipis, A.A. Yaremchenko, N.P. Vyshatko, A.L. Shaula, E.N. Naumovich, J.R. Frade, J. Solid State Electrochem. 7 (2003) 468.
[31] V.V. Kharton, A.L. Shaula, N.P. Vyshatko, F.M.B. Marques, Electrochim. Acta 48 (2003) 1817.
[32] P.S. Anderson, F.M.B. Marques, D.C. Sinclair, A.R. West, Solid State Ionics 118 (1999) 229.
[33] J. Mizusaki, I. Yasuda, J. Shimoyama, S. Yamauchi, K. Fueki, J. Electrochem. Soc. 140 (1993) 467.
[34] I. Kosacki, V. Petrovsky, H.U. Anderson, J. Electroceram. 4 (2000) 243.
[35] P. Kofstad, Nonstoichiometry, Diffusion and Electrical Conductivity in Binary Metal Oxides, Wiley-Interscience, New York, 1972.